Self-Assembling Semiconducting Polymers—Rods and Gels from Electronic Materials

Andrew P.-Z. Clark,[†] Chenjun Shi,[†] Benny C. Ng,[†] James N. Wilking,[†] Alexander L. Ayzner,[†] Adam Z. Stieg,[‡] Benjamin J. Schwartz,[†,‡] Thomas G. Mason,[†,‡] Yves Rubin,[†,*] and Sarah H. Tolbert[†,‡,*]

[†]Department of Chemistry and Biochemistry and [‡]California NanoSystems Institute, UCLA, Los Angeles, California 90095, United States

ABSTRACT In an effort to favor the formation of straight polymer chains without crystalline grain boundaries, we have synthesized an amphiphilic conjugated polyelectrolyte, poly(fluorene-*alt*-thiophene) (PFT), which self-assembles in aqueous solutions to form cylindrical micelles. In contrast to many diblock copolymer assemblies, the semiconducting backbone runs parallel, not perpendicular, to the long axis of the cylindrical micelle. Solution-phase micelle formation is observed by X-ray and visible light scattering. The micelles can be cast as thin films, and the cylindrical morphology is preserved in the solid state. The effects of self-assembly are also observed through spectral shifts in optical absorption and photoluminescence. Solutions of higher-molecular-weight PFT micelles form gel networks at sufficiently high aqueous concentrations. Rheological characterization of the PFT gels reveals solid-like behavior and strain hardening below the yield point, properties similar to those found in entangled gels formed from surfactant-based micelles. Finally, electrical measurements on diode test structures indicate that, despite a complete lack of crystallinity in these self-assembled polymers, they effectively conduct electricity.

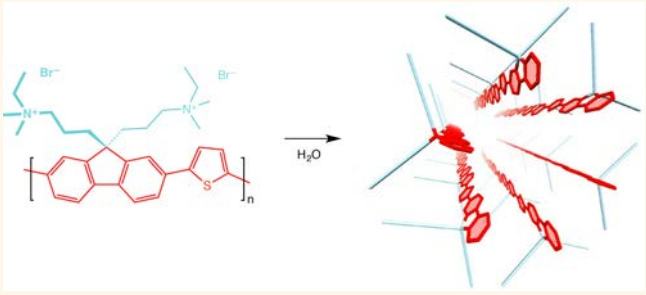

KEYWORDS: semiconducting polymer · amphiphilic assembly · self-assembly · hydrogel · polymer micelle · water-soluble conjugated polymer

Conjugated polymers have many potential applications in electronic and photonic materials as organic semiconductors.[1−8] They conduct electricity and are soluble in common solvents, facilitating processing by printing or thin-film deposition and patterning. Recent research has led to functional devices of many types, including fluorescent sensors,[3,9,10] transistors,[4,11,12] light-emitting diodes (LEDs),[1,13,14] lasers,[5,15−17] and photovoltaic cells.[2,6,18−21] In order to improve the properties of electronic devices incorporating conjugated polymers, considerable effort has been devoted to understanding the factors that influence the bulk conductivity and attempting to optimize them.

Since the intrinsic density of free charge carriers in most conjugated polymer systems is negligible and the injection barriers in most devices are sufficiently low, space-charge limited conduction (SCLC) is assumed, meaning that the electric field due to neighboring carriers dominates over the field due to the applied bias. Various models have been proposed to explain the current−voltage characteristics of thin-film devices based on this idea, including SCLC with an exponential trap distribution or a hopping transport field.[22] In modified SCLC models, there are distributions of traps that lie lower in energy than the carrier transport states. Such traps might be created by kinks in the polymer chains, which interrupt the conjugation along the backbone. Minimizing the number of kinks in the polymer backbone should therefore maximize the conductivity. Similarly, in hopping transport models, conduction is facilitated by charge carriers hopping from one chromophore to a neighboring chromophore. This process has a strong dependence on the orientation and distance between chromophores, implying that optimizing the geometry and packing density of adjacent polymers also should maximize the conductivity.

Although there is still debate as to which model is the most accurate, measurements of the field dependence of the hole mobility

* Address correspondence to tolbert@chem.ucla.edu, rubin@chem.ucla.edu.

Received for review June 12, 2012 and accepted January 23, 2013.

Published online January 24, 2013
10.1021/nn304437k

in dialkoxy-substituted poly(phenylene vinylene)s, in combination with spatially resolved photoluminescence and Raman spectroscopies, have revealed that higher mobilities correlate with improved packing of polymer chains in coplanar geometries, and that lower mobilities are influenced by disruption of the packing geometry and the conjugation length.[23] The conduction in conjugated polymer-based devices can therefore be improved by forcing the polymers to adopt aligned, straight-chain conformations that lead to efficient packing in the solid state.

Ordered polymer conformations have been shown to increase the charge carrier mobility; therefore, one might expect that the charge transport properties of conjugated polymer thin films should be enhanced by increasing the solid-state crystallinity. This has been investigated by comparing the crystallinity and charge carrier mobility of spin-cast thin films of regioregular poly(3-hexylthiophene) (P3HT) with different molecular weights (MW).[24] Surprisingly, the results showed that higher degrees of crystallinity correlate with lower mobilities.[24] This counterintuitive relationship results from the higher grain boundary resistance in more crystalline films. Poor overlap between crystalline domains and/or crystal faces with exposed insulating side chains inhibits the transport of charges between grains. Higher-MW P3HT films are less crystalline and possess higher overall mobilities because there are fewer grain boundaries. Because the polymer chains are longer than the crystalline domains, they can form bridges between neighboring grains, creating more continuous conductive pathways. Taken together, these results indicate that controlling both polymer chain conformation and domain structure is a worthy goal in the field of organic electronics.

One route used previously to gain a high level of control over polymer morphology has been to incorporate conjugated polymers into rigid matrices. For example, porous matrices can be made by templating inorganic phases such as silica using surfactants or block copolymers. Polymers can then be incorporated into these pores by diffusion or by *in situ* polymerization of infused monomers.[25−27] The pore size is found to influence the degree of interchain electronic communication, enabling control over polaron production, photoluminescence quantum yield, and charge carrier lifetime.[28,29] Related host/guest systems also can be produced by directly mixing a semiconducting polymer or monomer with the surfactant template prior to inorganic/organic coassembly.[30,31] The use of such host−guest systems, however, significantly impedes the processability of semiconducting polymers.

Another option for controlling structure and chain conformation in all-solution-based semiconducting polymer-based materials is to employ molecular self-assembly. A range of rod−coil diblock copolymers has been synthesized using semiconducting polymers for the rod block.[32−35] These diblocks have been shown to assemble into a rich array of nanoscale architectures.[32−35] Various combinations of nucleated growth and controlled aggregation have also been used to produce nanowires and nanocrystals from pure semiconducting polymers.[36−39] In most cases, the polymer backbone runs perpendicular to the long axis of the polymer nanofiber,[40,41] but in a few cases, fibers have been produced where the polymer chain axis is parallel to the nanofiber axis.[42]

In this work, we focus on amphiphilic semiconducting polymers as a route to obtain well-defined nanoscale structures. There is a rich literature on semiconducting polymers that have charged side chains (also termed semiconducting polyelectrolytes) similar to the ones described here. Polymers have been synthesized with anionic,[43−56] cationic,[44−62] or zwitterionic[63,64] side chains, combined with a diverse set of homopolymer or copolymer backbones. Many semiconducting polyelectrolytes have been synthesized since water-soluble chromophores form the basis for a large family of luminescence-based biosensors.[43,65−70] They also have been used extensively to modify charge injection barriers at interfaces.[46,71,72] We note, however, that despite the fact that both side chains and backbones similar to those used here have been made before, the previously reported charged polymers do not have a molecular geometry that is optimized for micelle formation, as we describe below.

Here, we build on this rich literature by reporting the synthesis and characterization of an amphiphilic poly(fluorene-*alt*-thiophene) (PFT) that serves as a self-assembling semiconductor. Specifically, our goal was to create a polymer that forms wire-like cylindrical micelles that can enable high conductivity by aligning the conducting axis of the polymer with the micelle axis. Like many of the charged polymers mentioned above, our PFT has cationic quaternary ammonium side chains, but the sp^3-hybridized bridging carbon on each fluorene unit allows for the incorporation of two charged groups on every repeat unit that are distributed radially from the plane of the polymer. The increased polar volume dramatically enhances solubility and is nearly ideal for creating a "pie-wedge" shaped building block that can easily assemble into a cylindrical micelle in polar solvents[73] (Scheme 1). Although both the fluorene and the thiophene comonomers contain nonlinear five-membered rings, the angles between the fluorene linkers and the thiophene linkers are complementary, giving rise to an approximately linear overall structure that further promotes the formation of cylindrical micelles. In designing this polymer, we also took into consideration the desired goal of enhancing visible light emission and absorption. The charged fluorene comonomer was chosen because of the need for a sp^3-hybridized carbon, while the thiophene comonomer was chosen both to create a straight polymer chain and to shift the blue fluorene absorption and photoluminescence into the visible

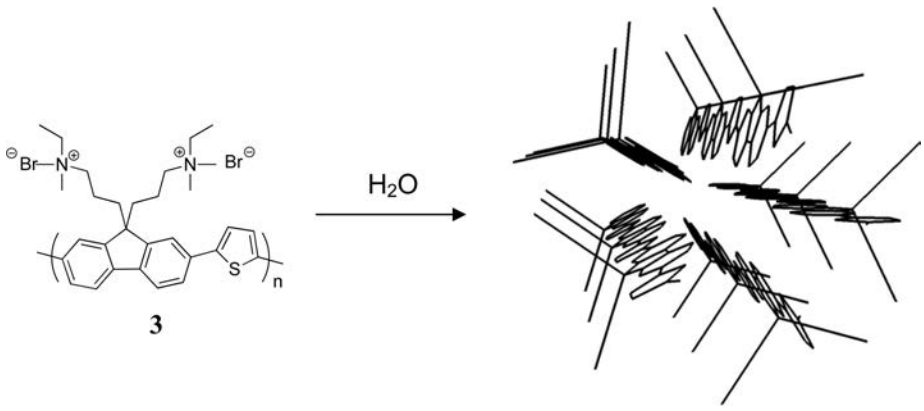

Scheme 1. Structure and self-assembly of PFT 3 micelles.

region. We note that the structure in Scheme 1 is not meant to be precise but rather merely suggestive of the general micelle structure. The side chains are not rigid and instead are highly disordered, and molecular detail has been omitted from the side chains in the scheme for clarity. The polymer backbones may also form some transient π-stacks with their neighbors, but the exact nature of those interactions is unknown.

The result of all of these considerations is a visible-emitting semiconducting polyelectrolyte that is highly soluble in water, a solvent that is ubiquitous, economical, environmentally responsible, and strongly promotes self-assembly. As we show below, PFT is able to form cylindrical micelles in aqueous solution, potentially increasing its ability to conduct efficiently over long distances. At high concentrations, PFT reversibly forms gels whose rheological properties suggest that they are composed of connected networks of semiflexible polymer fibers. The structure is thus nearly ideal for the formation of a three-dimensional conductive polymer network.

RESULTS AND DISCUSSION

In this work, the fluorene–thiophene copolymer [poly{(9,9-bis(3′-(*N*,*N*-dimethylamino)propyl)fluorene)-2,7-diyl-*alt*-(thiophene-2,5-diyl)}] (**2**) was first synthesized. This hydrophobic polymer was then converted to an amphiphilic polymer by quaternizing the dimethylamino side chains using bromoethane. The resulting polymer (**3**, PFT) was soluble in water and highly polar organics such as DMSO. Scheme 2 illustrates the synthetic method and proved structures for **2** and **3**. Two different batches of PFT **3** were synthesized in order to study the effects of the degree of polymerization on the self-assembly. As determined by gel permeation chromatography (GPC), the shorter polymer had a weight average molar mass M_w = 21 300 g/mol and polydispersity index of M_w/M_n = 2.02, while the longer polymer was approximately twice as long, having M_w = 35 000 and PDI = 1.75. According to the molecular model shown in Scheme 3, the average length of a monomer unit is approximately 12.4 Å, so

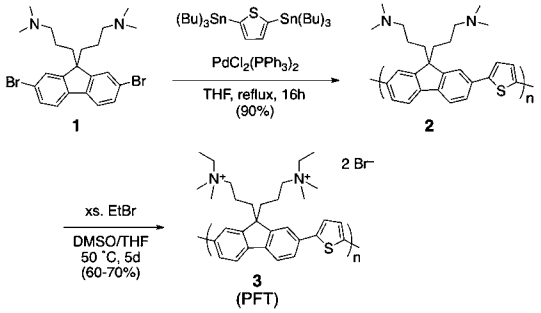

Scheme 2. Synthesis of amphiphilic poly(fluorene-*alt*-thiophene).

that when elongated, the low MW polymer chain would have an average mass weighted length of ~60 nm, while the high MW polymer would have an average mass weighted length of ~105 nm.

Solution-Phase Structural Studies. In determining whether macromolecular systems self-assemble in solution, two distinct questions must be addressed. The first question is simply whether molecular aggregates form, and the second concerns the specific structure of the aggregates. Here we use visible light scattering to assess the presence of aggregates in solution and synchrotron-based small-angle X-ray scattering (SAXS) to determine aggregate structure.

Before examining the data, we first consider the structures that are likely to form. In the present study, we have tried to produce a system optimized for cylindrical micelle formation. Both the fluorene and thiophene monomer units induce a bend in the polymer's backbone, which offset each other in the copolymer, allowing it to have a nearly straight backbone. This molecular geometry, shown in Scheme 3, was obtained using simple molecular mechanics.[63] Although the structure is not meant to be definitive, it does indicate that a straight polymer backbone, which is required for efficient micelle formation, is achievable with the polymers used here. The slight bend in the molecule observed in Scheme 3 may be caused by the finite nature of the oligomer employed in the calculations or may be a real feature of the optimized structure. Regardless, our goal is

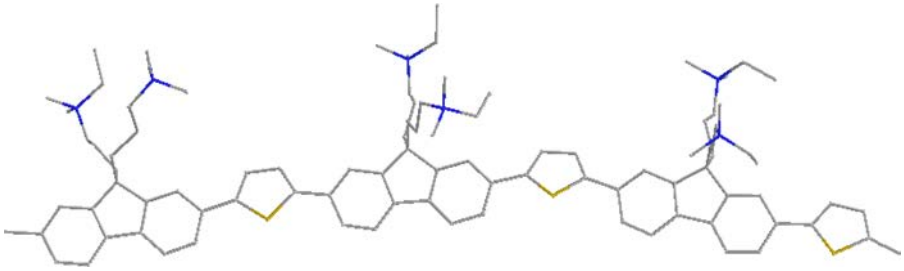

Scheme 3. Three-dimensional model showing nearly linear conformation of the PFT chain.

that the mostly straight nature of the polymer backbone will allow the system to form micelles, which in turn should prevent the coil formation that usually occurs for polymers in solution. It is known that solution-phase coiling can be preserved in the solid state, affecting electronic properties of solution-cast polymer films.[74]

Another important feature of PFT **3** is the fact that the sp^3-hybridized bridging carbon atom on the fluorene unit is used to attach solubilizing charged side chains. Because of the high propensity for π-stacking in semiconducting polymers, many polymer aggregates and nanowires contain some layered π-stacking motif.[40−42] The large polar volume of the quaternary ammonium groups on polymer **3**, however, produces a monomer unit that has a shape similar to a pie wedge. Amphiphilic molecules with a large polar volume and a small hydrophobic volume do not pack easily into layered structures but are able to efficiently fill space by assembling into a cylindrical micelle.[60] All of these design considerations thus give copolymer **3** the potential to make soluble, linear aggregates.

The scattering data presented in Figures 1 and 2 were collected on low-MW PFT samples because higher-MW samples tended to form larger assemblies in solution with more inhomogeneity and thus could not be structurally characterized with sufficient rigor. As discussed below, some of the higher-molecular-weight samples can form hydrogels, but none of the samples used in our light or X-ray scattering studies gel at any accessible concentration. These studies are thus aimed at examining the simplest aggregate structures that form in solution. We begin with dynamic light scattering (DLS), which can be easily performed in a range of aqueous and organic solvents. The concentration of all samples was maintained at 10 mg/mL, which provided optimal scattering intensity, and the data were fit to single-exponential (unimodal) functions. Such single-exponential fits are equivalent to assuming that spherical aggregates are formed in solution. Unfortunately, higher-level fits that directly model shape anisotropy could not be uniquely fit to the data because of the combination of shape anisotropy and polydispersity. Some information about aggregate shape can be obtained from angle-dependent data, however. For example, a trend of decreasing apparent size with increasing scattering angle, as observed in Figure 2,

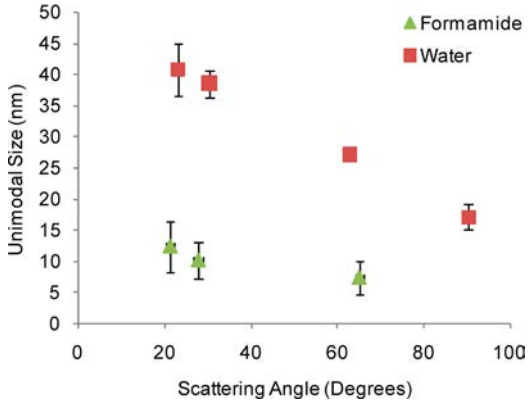

Figure 1. Dynamic light scattering (DLS) of PFT 3 dissolved in water and formamide as a function of scattering angle. Larger particle sizes in water and decreasing apparent sizes with increasing scattering angles indicate that the particles have asymmetric shape, consistent with a cylindrical micelle model. In formamide, smaller sizes with larger standard deviations indicate small, amorphous aggregates or molecularly dissolved polymer chains.

indicates that the particles have an anisotropic shape.[75] We note that because our model describes anisotropic particles with a spherical particle that has the same average diffusion constant, the numerical size presented in Figure 1 is neither the length nor the diameter of the anisotropic aggregate but is instead something between the two.

Figure 1 shows DLS data on PFT **3** dissolved in solutions of water and formamide at 10 mg/mL. Much larger aggregates are observed in water (∼20−40 nm), compared to formamide (∼7−12 nm), indicating that the polymer self-assembles in water but not in formamide. The angle-dependent data for water also show a systematic decrease in apparent size with increasing angle, consistent with an anisotropic self-assembled structure in aqueous solution. By contrast, the smaller particles formed in formamide are consistent with molecularly dissolved or minimally aggregated polymer chains in a loose random coil conformation. These data are consistent with our understanding of amphiphilic assembly in hydrogen-bonded liquids. Disruption of hydrogen bonds in network-forming solvents like water by dissolution of nonpolar organic groups comes at a large energetic cost, thus providing the driving force to bury the nonpolar groups in the cores of spherical or cylindrical micelles.[76]

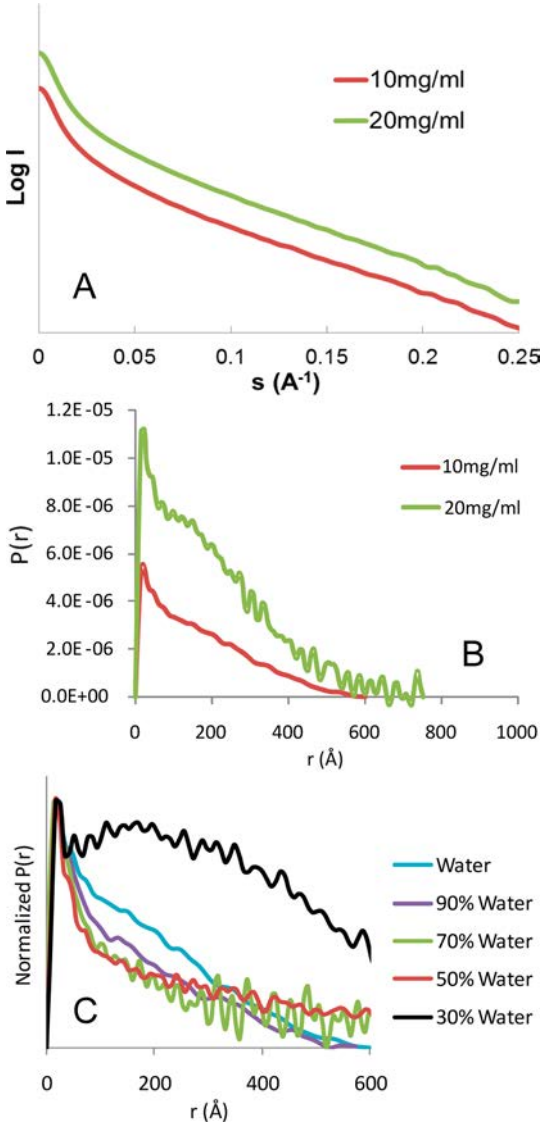

Figure 2. Small-angle X-ray scattering (SAXS) data for PFT 3 solutions. (A) Raw SAXS data collected on PFT 3 in aqueous solution. (B) *P*(*r*) curves for aqueous PFT 3 solutions obtained by Fourier transformation of the data in part A. The data show cylindrical scattering profiles at both 10 and 20 mg/mL. Cylindrical micelles have diameters of ~4 nm and scattering intensity proportional to concentration. (C) *P*(*r*) curves for PFT 3 dissolved in a mixed solvent system with various volume ratios of water (good solvent) to ethanol (poor solvent) all at 10 mg/mL. Addition of poor solvent maintains cylindrical micelles until EtOH concentration increases to 70%, at which point cylinders coexist with globular aggregates.

X-ray Scattering. In order to gain more quantitative information on the size and shape of the PFT aggregates in solution, we performed small-angle X-ray scattering (SAXS) measurements using a synchrotron radiation source. The raw data (Figure 2A) were converted by Fourier analysis to *P*(*r*), an electron distribution function which represents the radially averaged distribution of electron density correlations as a function of the separation distance *r* within a given solution-phase aggregate (Figure 2B,C). The *P*(*r*) data therefore yield information about the scattering form factor of the dissolved particles, and since motional averaging reduces interparticle correlations, the *P*(*r*) curve predominantly contains information about the average shape of the particles in solution. We note that if the interparticle spacing is correlated, such as in the case of liquid crystals or other aligned systems, peaks may also be observed that correspond to the average interparticle distance.

Figure 2A shows the wave-vector-dependent scattering data plotted for two different concentrations in aqueous solution. Fairly featureless data of this sort are expected for cylindrical micelles in solution.[77] Figure 2B shows *P*(*r*) curves obtained by Fourier transformation of the data in part A. The data for both 10 and 20 mg/mL solutions of PFT show typical cylindrical scattering profiles: a sharp peak that corresponds to correlations across the diameter of the cylinder, followed by a linear decay, ending in a baseline intercept that correlates with the cylinder length.[72] For these data, the X-ray detector used only allowed for two decades of range in scattering angle and hence two decades in distance. As a result, the baseline intercept may underestimate the actual length of the cylindrical particles. The observed radius of approximately 2 nm correlates well with molecular models of a structure like that shown in Scheme 1,[63] which show an end-to-end distance between the polymer backbone and side chains of approximately 1 nm. The baseline intercept of 60−70 nm is on the same order of magnitude as the particle size measured by DLS and is in excellent agreement with the mass weighted average polymer length of 60 nm. However, the signal-to-noise ratio near the baseline is low, and it is also near the minimum scattering angle (maximum particle size) of the detector in this experiment (100 nm), so this value might underestimate the actual length of the cylinders. Although the micelle length is not precisely determined in this experiment, the SAXS data presented in Figure 2B provide concrete structural proof that low-molecular-weight PFT **3** forms cylindrical micelles in aqueous solution and suggests that the micelle length in low-molecular-weight polymers may be dominantly determined by the average molecular weight of the polymer.

We note that, in the SAXS profiles, there is a broad peak centered at a distance of approximately 16 nm (160 Å) superimposed on the standard cylindrical scattering profile (Figure 2B). This peak grows in intensity and shifts to lower *r* in the higher-concentration sample, indicating that it may be an interparticle correlation peak. As discussed below, aggregate correlations lead to hydrogel formation in higher-molecular-weight versions of these polymers, and the correlations observed in Figure 2B are likely the first step in that process.

In order to determine the robustness of these micelles in non-aqueous solutions, we also performed SAXS experiments on PFT aggregates dissolved in mixed solvent systems consisting of various volume

ratios of water and ethanol. Because ethanol is only a weakly hydrogen-bonding solvent, it does not promote amphiphilic assembly nearly as well as water.[71] In addition, PFT **3** is much less soluble in ethanol than in water. All samples were dissolved at 10 mg/mL, and the volume percent of ethanol to water was varied from 10 to 70%. As shown in Figure 2C, cylindrical particles are maintained upon addition of EtOH until the volume fraction of EtOH in the solution reaches 70%, at which point the peak corresponding to the cylinder radius is still visible, but the cylinder scattering profile becomes convoluted with a broad peak, indicating the coexistence of cylindrical micelles with larger solution-phase aggregates.

Finally, while null data are not usually discussed in a scientific manuscript, it is worth ending this section with a brief discussion of high-angle diffraction obtained on films of these amphiphilic polymers. Polythiophene-based polymers tend to be highly crystalline,[78] but unlike most pure polythiophene derivatives, this amphiphilic copolymer shows no high-angle diffraction. That fact runs contrary to most of the current literature on polythiophene-based nanostructures[36,37] but is consistent with the general structure presented in Scheme 1, suggesting that amphiphilic interactions, rather than π-stacking, dominate the self-assembly of these materials.

Atomic Force Microscopy. Although the data above provide good evidence that PFT **3** forms cylindrical aggregates in solution, our ultimate goal is to make thin-film optoelectronic devices, so it is important to understand if these micellar structures can be transferred to the solid state with retention of the nanoscale structure. We thus employed atomic force microscopy (AFM) to image submonolayer films of low-MW PFT deposited on substrates. We found organized structures only in samples drop-cast from dilute solutions (0.01 mg/mL); samples cast from more concentrated solutions formed thick films with large agglomerates that could not easily be imaged (not shown). Films cast from more dilute solutions, however, showed submonolayer coverage with anisotropic polymer domains. Figure 3 shows a representative AFM image of a sample of PFT drop-cast on a mica substrate from a 0.01 mg/mL solution made of 90% water and 10% ethanol. Ethanol was added to aid wetting of the mica surface in order to produce more homogeneous films. Figure 3A shows a large-area image (5.7 $\times$ 5.7 μm) with multiple rod-like polymer aggregates on a thin layer of amorphous polymer underneath. Single rods and bundles of rods are visible, indicating that some micelles agglomerate during the drying process. Figure 3B shows a zoomed-in image (750 nm $\times$ 750 nm) of the large bundle indicated by the black square in the image in Figure 3A. Here, individual rods are clearly visible within the bundle.

The black lines in Figure 3A,B correspond to the height profiles in Figure 3C,D, respectively. The cross sectional height of the isolated rod in Figure 3A is 4.2 nm, while the heights of the rods within the bundle in Figure 3B vary from approximately 2.5 to 4.5 nm. Measuring height profiles of many different rods, both single and bundled, yields the histogram shown in Figure 3E. The observed rod heights of ~3−5 nm correlate well with the SAXS data, which indicates a cylinder diameter of approximately 4 nm. It should be noted that the in-plane widths of the rods are fairly consistent in the range of 15 nm. Although one would expect a circular cross section for the self-assembled PFT cylindrical micelles, this is not necessarily inconsistent with the height data because the in-plane measurement is convoluted by the finite width of the silicon tip of the AFM probe. The 15 nm value is thus a measure of the AFM tip diameter, rather than the in-plane micelle diameter. The height data are therefore more accurate, and the actual width of the rods is likely closer to the 3−5 nm observed height.

Micelle lengths tend to be several hundred nanometers, which is significantly longer than the 60 nm length observed by SAXS. It is not clear if this discrepancy is caused by restructuring or joining of the micelles upon evaporation, by bias in the SAXS measurement toward smaller structures, or by bending of the micelles in solution. If the latter is true, then SAXS measures the average persistence length of micelles in solution (~60 nm) and AFM measures the actual micelle length (hundreds of nanometers). What is clear from the AFM measurements is that micelles significantly longer than the average molecular weight *can* form by overlapping assembly of the polymer chains. That conformation is required for the gel formation discussed below.

Regardless of the precise length, the observation of rod-like particles in the solid state as well as in solution indicates that the amphiphilic structure of PFT **3** provides a strong tendency to self-assemble into cylindrical aggregates, and this structure is maintained when cast as a film. Preservation of the cylindrical micelles observed in SAXS in the solid state is a necessary prerequisite for the use of this self-assembled polymer in any electronic devices.

Polymer Rheology. In order to function efficiently in an electronic device, the PFT active layer must not only form local conductive pathways but it must also form a continuous network to allow for long-range conductivity. Moreover, cylinders lying in the plane of the film, like those shown in Figure 3, are not ideal for typical sandwich structure devices, where current must flow normal to the plane of the film. To address this, we consider the formation of gel networks from these polymers. Three-dimensional networks of thread-like molecules or aggregates swollen with aqueous solvent (hydrogels) can be formed from many types of molecules that assemble into linear aggregates, including surfactants,[79] polyelectrolytes,[80] and biopolymers.[81] These networks are formed when the concentration is high enough that the molecules or aggregates

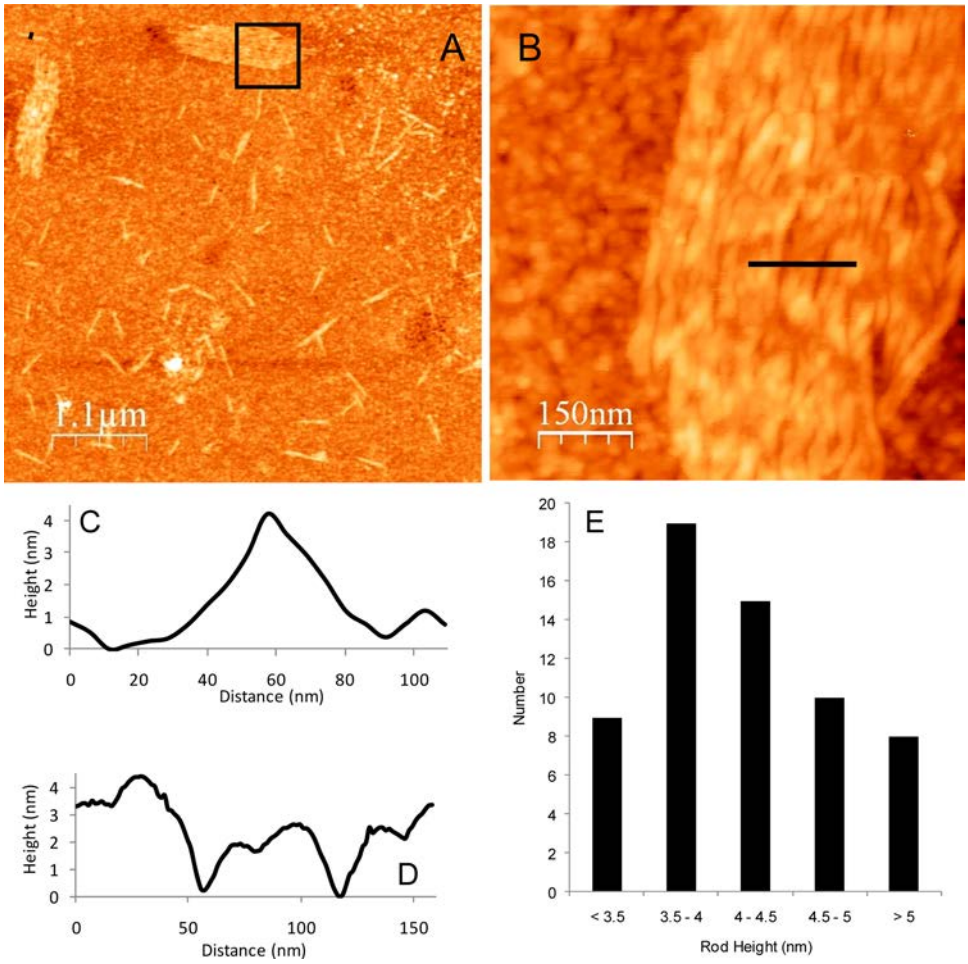

Figure 3. Atomic force microscope (AFM) images of PFT 3 on mica substrates showing rod-like aggregates (height scale = 12 nm). (A) 5.7 × 5.7 μm image showing individual rods and aggregated bundles of rods. (B) 750 × 750 nm image showing a zoomed-in image of the large bundle of rods indicated by the box in (A). (C,D) Cross sectional height profiles corresponding to the black lines in (A) (upper left corner) and (B), respectively. (E) Histogram of rod heights, showing an average around 4 nm, in agreement with cylindrical micelle diameter from SAXS.

become entangled (either physically or chemically) to form a percolating network, yielding viscoelastic gels.

We find that, depending on the degree of polymerization, high-MW PFT forms gels at aqueous concentrations of 1.5−2.5% by mass at room temperature. Figure 4 shows a picture of one of these gels in an inverted vial showing that neither the gel nor the embedded stir-bar flows under the force of gravity. Gel formation is reversible upon addition of solvent, but the gels are stable at elevated temperatures up to the boiling point of water.

The rheological properties of these gels were measured using a strain-controlled rheometer employing a cone-and-plate geometry. These properties are highly dependent on the concentrations of the starting solutions. Figure 5A shows the frequency-dependent elastic storage modulus G' and viscous loss modulus G'' of PFT gels at concentrations of 16 and 21 mg/mL. All data were collected at an amplitude of 1% strain. The data show that $G' > G''$ across most of the frequency range for both samples, indicating that the gels are indeed more solid-like than liquid-like. The moduli of the 21 mg/mL gel are nearly an order of magnitude greater than those of the 16 mg/mL gel, however. This dramatic increase in modulus for a relatively small increase in concentration suggests that the polymer micelles are strongly interacting in the gel network.

The characteristic relaxation time can be estimated from the crossover point of G' and G'' by simply extrapolating power law fits to the data and calculating the inverse of the frequency at which $G' = G''$. The characteristic relaxation time of approximately 8600 s (2.4 h) for the 16 mg/mL gel indicates that it flows very slowly. The characteristic relaxation time of about 43 000 s (11.9 h) for the 21 mg/ml gel is nearly an order of magnitude larger than that of the 16 mg/ml gel, reflecting the higher storage modulus of the more concentrated sample. The density of entanglements in the gel network can also be estimated from the frequency-dependent modulus data. The plateau modulus at intermediate frequencies G_p is related to the entanglement length L_e by $G_p = kT/L_e^3$.[82] By estimating G_p as G' at the inflection point[83] in the

Figure 4. Photograph of a PFT hydrogel suspended in a vial upside down, trapping a magnetic stir bar and showing the resistance to viscous flow by gravity.

intermediate frequency regime, the entanglement length is estimated to be ≈83 nm for the 16 mg/mL gel and ≈42 nm for the 21 mg/mL gel. The shorter length is consistent with the much stiffer gel observed at higher concentration. We note that a correlation distance of similar magnitude to these values was observed in SAXS (Figure 2), suggesting that the micelles may begin to entangle before gelation occurs.

Figure 5B,C shows strain-dependent dynamic storage moduli of dilute and concentrated PFT gels collected at a frequency of 5 rad/s. Both samples exhibited an increase in their storage moduli with increasing strain prior to the yield point, a phenomenon known as strain hardening (or strain stiffening). Such behavior is not generally observed in random polymer gels, but it has been observed in gels made from surfactant micelles with added salt[84] and in structural biopolymer gels.[85] These systems are both composed of semiflexible thread-like chains that form gels with entangled filaments having a finite extensibility and bending energy. This resistance to bending and stretching causes the material to harden as the strain is increased. The magnitude of strain hardening typically increases with increasing cross-link density, which is a function of the mass concentration of the gel.[80] This second trend is not observed in our PFT gels, which may be an indication that the micelle fibers are already fully extended in high-concentration gels. Although further study is clearly required to fully understand the behavior of the PFT gels, the key result is that the rheological data are fully consistent with a strongly interacting and dense network of semiconducting polymer fibers. On the basis of the SAXS and AFM results for lower-molecular-weight versions of PFT **3**, it is likely that polymer micelles form the basic building blocks of these gels.

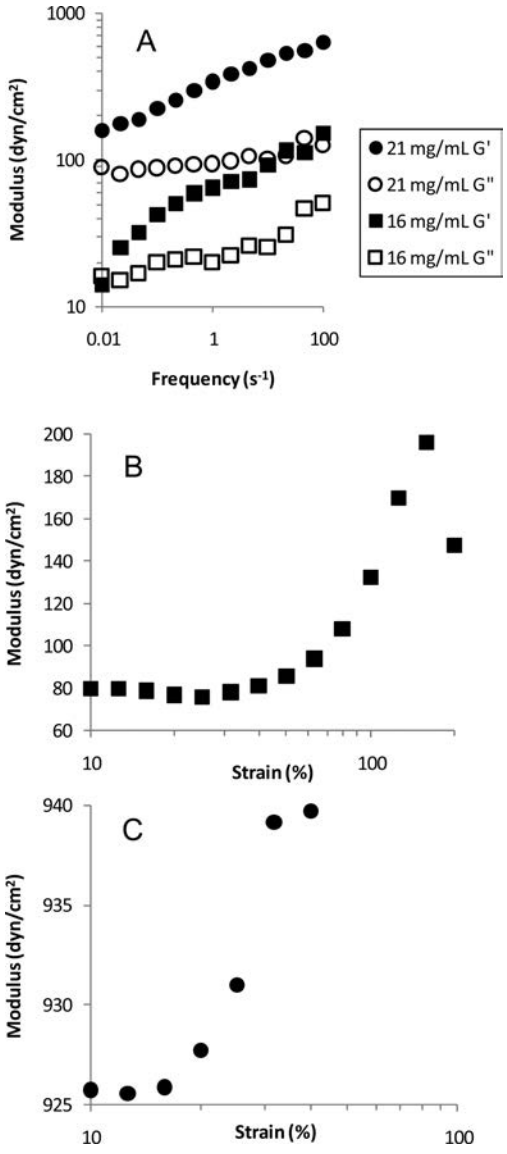

Figure 5. Rheological properties of PFT 3 gels formed spontaneously in aqueous solution as a function of concentration. Gel formation is reversible upon dilution, and recovery is rapid, as rheology is not affected by cycling or yield history. (A) Frequency-dependent storage (G') and loss (G'') moduli for gels formed from PFT 3 solutions of 16 and 21 mg/mL. $G' > G''$ indicates a gel or solid-like material. Estimated plateau moduli and crossover points of G' and G'' indicate that the higher-concentration sample has a smaller entanglement length and longer characteristic relaxation time. (B) Storage modulus G' as a function of strain for 16 mg/mL gel. Strain hardening suggests that the gel is composed of entangled semiflexible polymer micelle filaments. (C) Storage modulus G' as a function of strain for ∼22 mg/mL gel. Here the modulus is higher, but less strain hardening occurs.

Optical Properties. As discussed above, the fluorene monomer is an important building block of this amphiphilic polymer because of the need for an sp^3 carbon to join the charged side chains to the polymer backbone in a noncoplanar geometry. Fluorene is not, however, an ideal monomer to use in organic photovoltaic cells. With a band gap of 2.95 eV,[86] the

absorption of polyfluorene lies in the blue and ultraviolet range of the spectrum, providing poor overlap with the peak of the solar spectrum. Polythiophene, by contrast, has a moderately small band gap of 2.1 eV,[87] providing a somewhat better match with the solar spectrum. By copolymerizing fluorene with thiophene, we are able to shift the band gap to longer wavelengths, while maintaining the needed sp^3 side chain attachment site. The band gap of PFT was determined by comparing the optical absorption spectra of several films of varying thicknesses (data not shown) in order to correct for optical scattering. The divergence point between the spectra of various film thicknesses was assigned as the band gap. Our measured band gap of 2.50 eV is the same for both low- and high-molecular-weight samples and is quite close to the average of the reported polyfluorene and polythiophene band gaps.

In general, the photophysical properties of PFT **3** were independent of the degree of polymerization, and so all data presented in Figure 6 correspond to the higher molar mass sample in order to maintain continuity between solution, film, and gel samples. Figure 6A shows absorption and photoluminescence (PL) spectra of PFT in two different solvents: water (which promotes assembly) and formamide (which does not). There are a number of issues to consider in correlating polymer chain conformation with photophysics.[88] Straighter polymer chains should have a longer average conjugation length, leading to red-shifted absorption and emission. Bringing polymer chain segments into close contact can also lead to the formation of low-energy interchain delocalized excited-state species or simply provide a higher dielectric constant environment for each chromophore, either of which can again result in a red shift of the emission.[89] As indicated by SAXS, in PFT **3**, the linear polymer backbone, combined with the highly amphiphilic nature of the polymer, causes the polymers to form micellar aggregates like those shown in Scheme 1. In this case, both chain conformation and aggregation should favor red-shifted absorption and luminescence. By contrast, DLS indicates that little aggregation takes place in formamide, and so the polymer chains should be molecularly dissolved and likely coiled. In agreement with these ideas, both absorption and PL are red-shifted in water compared to formamide. The difference in the magnitude of the peak shift in absorption (14 nm) and PL (8 nm) likely results from solvatochromism, which depends on the dipole moments of the ground and excited states.[90]

Beyond spectral shifts, previous research on conjugated polymers also has shown that aggregation can cause changes in the structure of the optical absorption and emission spectra.[1,91,92] In PFT **3** (Figure 6A), only one peak is evident in the absorption spectrum in formamide (421 nm), but the appearance of a red shoulder produces two peaks in water (435 and ~471 nm). This red shoulder has been associated with polymer aggregates containing linear polymer chains, and it is usually assigned either to

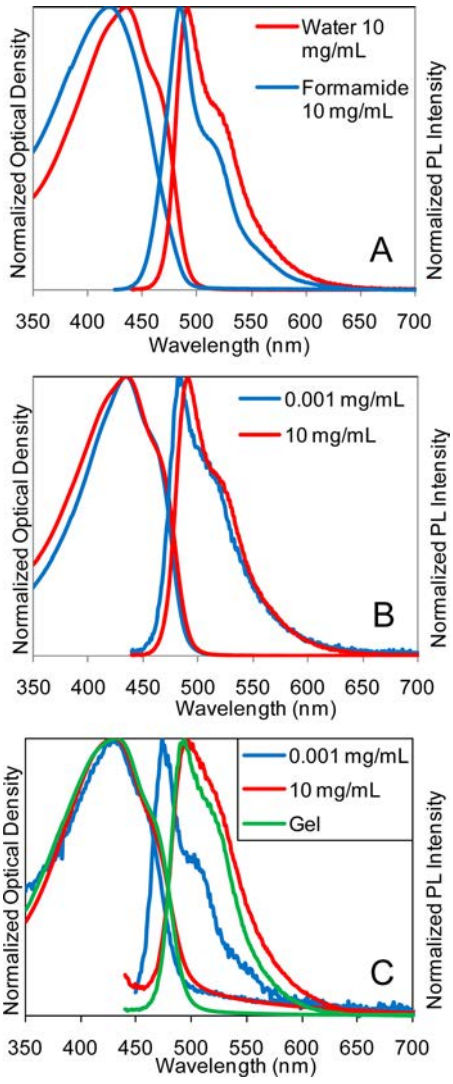

Figure 6. Optical absorption and photoluminescence spectra of PFT 3 normalized to show spectral shifts. (A) PFT 3 in water and formamide solution. PFT 3 self-assembles to form cylindrical micelles in water but not in formamide. (B) Aqueous solutions of PFT 3 at high and low concentrations. (C) Thin films cast from the two aqueous solutions shown in part B. A polymer gel made from PFT 3 is included for comparison.

enhanced vibronic structure or to an interchain excited state.[93] In the luminescence, two peaks are evident in both solvents (490 and 521 nm in water, 482 and 511 nm in formamide), but the magnitude of the lower-energy peak is increased in water. The energy difference between these two peaks correlates well with the vibronic structure that arises from the excited-state displacement of the C=C stretch in other conjugated polymers.[1,86] The increased vibronic shoulder in the aqueous sample is also consistent with micelle formation in water but not in formamide because increased vibronic coupling is favored in straight-chain conformations.

By analogy to other amphiphilic systems, such as surfactants and block copolymers, it would be reasonable to assume that the formation of PFT **3** micelles also

depends on the solution concentration,[94] and that spectral differences similar to those observed in water and formamide could be tuned using concentration. Figure 4B shows optical absorption and emission spectra of PFT in aqueous solution at 0.001 mg/mL (near the lower limit of observable optical density) and 10 mg/mL. The absorption and PL spectra are similar at both concentrations, indicating that the polymer is assembled at all measurable concentrations.

Although concentration-independent assembly of conjugated polyelectrolytes has been observed before,[95] it is worth considering why this occurs. For most molecular amphiphiles, there is a critical micelle concentration (CMC) below which the amphiphilic molecule dissolves in monomeric form. The CMC is determined by the interplay between the enthalpic price associated with disruption of the water hydrogen-bonding network by dissolution of a nonpolar group in water and the entropic price associated with aggregating many surfactant molecules into a single micellar species. Because PFT is a facially amphiphilic polymer, the enthalpic price for exposing the nonpolar backbone to water should be high, and the entropic loss associated with self-organization should be small compared to a monomolecular species like a surfactant. Therefore, the CMC is likely to be exceedingly low for these materials.

Figure 6C shows the optical absorption and PL spectra of PFT **3** thin films cast on glass substrates from aqueous solutions of various concentrations of the polymer. The absorption shifts in these spectra reveal changes in the conformations of the polymer chains in different solid-state environments, even when cast from solutions with similar absorption. The film cast from dilute solution (0.001 mg/mL) shows an absorption peak position (433 nm), which is similar to the aqueous samples, but the primary peak in the PL spectrum is blue-shifted (475 nm). The AFM data in Figure 3 show a similar sample cast from low-concentration solution to consist of submonolayer coverage of micelles, well separated from each other in most cases. Polymer rearrangement upon drying or micelle substrate interactions may result in the blue-shifted PL, and the fact that micelles are not interacting prevents energy transfer between micelles that could result in redder PL.

Solutions up to 10 mg/mL can be similarly used to generate solid-state film samples using spin-coating or drop-casting. Increasing the concentration further beyond the gel point (16 mg/mL) results in the formation of a viscoelastic hydrogel. Gel samples were prepared for absorption and photoluminescence measurements by compressing a small amount (~10 μL) of gel between two glass coverslips and sealing the edges with vacuum grease to avoid excessive evaporation of water in the hydrogel during the measurements. For both films cast from high-concentration solutions (10 mg/mL) and for gel samples, the data are similar

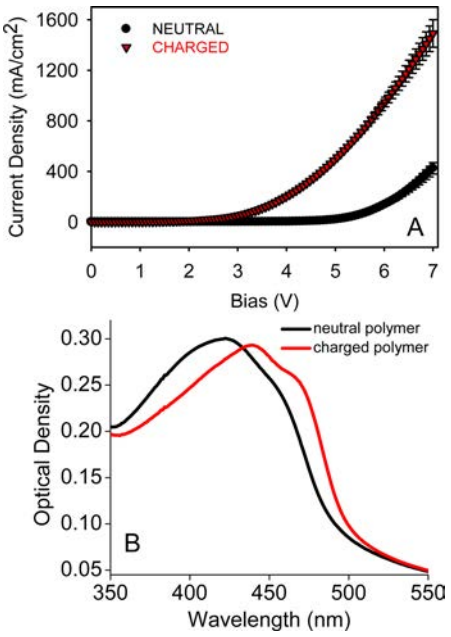

Figure 7. (A) Current–voltage characteristics for both charged and uncharged versions of PFT 3. Significantly higher current densities are observed in the charged, micelle-forming polymer, indicating a higher carrier mobility in this polymer. (B) UV/visible absorption for the devices used in part A. The absorption of the neutral polymer is blue-shifted with respect to the charged analogue, indicative of a more coiled chain conformation.

(Figure 6C). The absorption and luminescence are both very similar to the solution-phase spectra in terms of peak position and shape. These data thus add weight to the argument that aggregates present in solution are preserved in the solid state and in gel samples.

Current–Voltage Characteristics. The experiments listed above all suggest that the amphiphilic PFT **3** described in this work forms cylindrical micelles in solution, and the micelle structure is preserved in the solid state and in gel networks that form upon concentration. In order for these self-assembling polymers to find eventual device applications, however, a fundamental question that we must address is whether the high density of positive charges on the side chains inhibits electrical conductivity in these materials. Although direct mobility measurements are beyond the scope of this work, we have constructed bipolar diodes from the high-MW amphiphilic PFT **3** described above. Figure 7A shows the diode response of a PFT film cast onto a PEDOT:PSS-coated ITO substrate. The diode uses a vapor-deposited aluminum cathode, and the device was thermally annealed prior to cathode deposition. We find that PFT can support reasonable current densities, indicating that it could potentially be used in device applications. The simple fact that a high density of permanent charges, a novel self-assembled architecture, and little or no π-stacking do not inhibit electrical conductivity is the most important conclusion of this section.

It is also interesting to compare the behavior of PFT to the same polymer (**2**) before quaternization of the side chains in an effort to see how self-assembly modifies the conductivity of polymer **3**. The uncharged parent polymer **2** does not assemble in standard organic solvents and thus serves as a control for the effect of self-organization since the two polymers have identical backbones and thus identical electronic structures. We have verified that the thicknesses of the two polymer films are similar by profilometry and UV–visible absorption spectroscopy (Figure 7B). Figure 7A indicates that the amphiphilic polymer **3** supports a current density that is roughly 4 times greater than its neutral analogue **2** at a forward bias of 7 V. This is consistent with the expectation that the charge carrier mobility should be higher in a system with straight polymer chains. Carrier traps can form when a chain kinks and breaks the π-conjugated network.[96,97] Straight chains should have a lower density of traps and thus a higher carrier mobility. Therefore, all else being equal, both drift and diffusive carrier motion should be enhanced in the strongly assembling conjugated polyelectrolyte. This conclusion is supported by the UV–visible absorption spectrum, shown in Figure 7B, which highlights the differences between the charged and neutral polymer films. The spectrum of the polyelectrolyte is clearly shifted to redder wavelengths relative to the neutral polymer. Coiling of polymer chains leads to shorter conjugated segments and thus causes both the blue shift in the absorption and the increased trap density discussed above.[98,99]

There is, however, a complication that arises when assessing the intrinsic electronic conductivity of polyelectrolytes because of electrode–ion interactions. Specifically, counterions distributed along the polymer backbone can migrate under the influence of an applied bias.[58] This ion motion could work to screen the electric field at the metal–organic interface, lowering the effective interfacial potential energy barrier and consequently allowing charge injection to take place from metal electrodes with Fermi levels that are energetically mismatched relative to the HOMO and LUMO levels of the polymer.[59] The dynamic signature of this screening effect is a current density that increases monotonically with time until a plateau region is reached.[58] Previous work employing thin semiconducting polyelectrolyte interface layers showed response times on the order of 10 s using organic counterions.[58] To probe whether a similar phenomenon is affecting current densities in our bulk amphiphilic polymer diodes, we measured the current–voltage characteristics of our PFT diodes at two different integration rates, one faster than the characteristic ion motion time reported previously (~1 s) and one comparable to previously reported response times (~10 s). As shown in Figure S3 in the Supporting Information, we find no enhancement in the injected current magnitude with sequential scans or slower integration rates. We thus conclude that dynamic ionic redistribution under applied bias is not an important effect in our system, a result that is consistent with previous studies when Br^- was used as a counteranion.[58]

We note that, in addition to dynamic ion effects, there is also the possibility that static dipoles at the interface, which are present in the charged polymer but not in the neutral control polymer, could modify carrier injection barriers, allowing for higher current densities in our amphiphilic PFT **3**. Although we have no quantitative way to assess the effect of these interfacial dipoles, we find that a log–log plot of the data shown in Figure 7A produces a much higher slope for the neutral polymer **2** than the charged PFT **3**. A variety of modified space-charge-limited current models indicate that transport that occurs within a manifold of trap states will produce a higher slope in a log–log J–V plot. Thus, while these models do not allow us to extract mobilites for either polymer, the data are consistent with our picture of a lower trap density in the self-assembled, micelle-forming polymer **3**.[100] Therefore, it appears reasonable that the differences we observe between the amphiphilic polyelectrolyte **3** and its neutral analogue **2** in Figure 7A are due at least in part to differences in the intrinsic charge conductivity and do not arise solely from modified injection barriers.

CONCLUSIONS

We have designed and synthesized a water-soluble conjugated polyelectrolyte (PFT **3**) as an active material for optoelectronic applications. Like many semiconducting polymers, PFT **3** can be processed in solution, but aqueous solubility eliminates the need for organic solvents, which are less economical and environmentally responsible, particularly in roll-to-roll processing, which generates significant solvent vapor. By incorporating alternating thiophene monomers with water-solubilizing fluorene monomers, the optical band gap of the polymer is shifted into the visible region of the electromagnetic spectrum, giving it the potential for applications in photovoltaics or visible light-emitting diodes. In order to improve carrier mobility in this polymer, we designed PFT **3** to self-assemble into cylindrical micelles containing fully extended polymer chains. DLS and SAXS indicate that the polymer indeed forms cylindrical micelles in solution, and the structure of these micelles can be preserved in the solid state, as observed by AFM. Films and solutions of this assembling semiconducting polymer show red-shifted luminescence and absorption, consistent with a fully extended chain conformation.

At high enough concentrations, PFT reversibly forms entangled hydrogels. Strain-controlled oscillatory rheological measurements indicate that these gels have solid-like properties, and that they can display a high degree of strain hardening. These properties are

similar to the rheology of other systems consisting of entangled networks of filaments with finite extensibility and bending energy. This network of semiflexible conjugated polymer micelles should have conductivity in three dimensions, making it an exciting system for optoelectronic applications. In agreement with this idea, current−voltage measurements indicate that the micelle-forming PFT **3** can support a much higher current density than the control polymer **2** that has the same conjugated backbone but does not possess charged side chains.

The self-assembling, network-forming polymer **3** has interesting potential for optoelectronic applications. In addition to the environmental advantages of a water-processable semiconducting polymer, the three-dimensional network formed by the PFT **3** gels potentially could also be used in chemical sensing applications.[101−104] Although charged polymers have been extensively employed as chemical sensors, the vast majority of work to date is optically detected, and a fully interconnected gel network could enable electrically detected sensors. This system thus holds interesting potential for conventional optoelectronic devices, as well as for new applications made possible by the self-assembly and gelation properties of this network-forming semiconductor.

EXPERIMENTAL DETAILS

Polymer Synthesis and Quaternization. 2,7-Dibromo-9,9-bis(3′-(*N*,*N*-dimethylamino)propyl)fluorene and 2,5-bis(tributylstannyl)-thiophene were synthesized according to published procedures.[57,105]

Poly{(9,9-bis(3′-(N,N-dimethylamino)propyl)fluorene)-2,7-diyl-alt-(thiophene-2,5-diyl)} (2). 2,7-Dibromo-9,9-bis(3′-(*N*,*N*-dimethylamino)propyl)fluorene (494 mg, 1.0 mmol), 2,5-bis(tri-*n*-butylstannyl)-thiophene (662 mg, 1.0 mmol), dichloro(bistriphenylphosphine)-palladium (14 mg, 0.02 mmol), and anhydrous THF (30 mL) were placed in a 100 mL three-necked flask equipped with a magnetic stirrer and condenser. The system was purged with argon, and the mixture was gently refluxed for 16 h. Some precipitate was observed at the end of the polymerization. To terminate the polymerization, hexane was added to the mixture. The precipitated polymer was separated by filtration and then washed with distilled MeOH, followed by hexanes, which was sufficient to remove the palladium catalyst (no PPh_3 or Ph_3PO by ^1H NMR). The polymer was not fractionated for these experiments. After drying under vacuum, polymer **2** was obtained as a yellow powder (430 mg, ∼90%): ^1H NMR (500 MHz, $CDCl_3$, Figure S1) δ (ppm) 0.82−0.78 (m, 2H relative integration), 2.02 (m, 16H), 2.14 (m, 4H), 7.38 (m, 2H), 7.62−7.50 (m, 2H), 7.65 (m, 4H), 7.72−7.68 (m, 2H).

*Quaternized Polymer (**3**, PFT).* A 100 mL flask with a magnetic stir bar was charged with the neutral polymer (430 mg) dissolved in 40 mL of THF. To this were added a large excess of bromoethane (5 mL) and 20 mL of DMSO. The solution was stirred at 50 °C for 5 days. The THF solvent and excess bromoethane were then evaporated. The polymer was precipitated with 100 mL of ethyl acetate, collected by centrifugation, washed with chloroform and THF, and dried overnight under vacuum at 60 °C: yield 60−70%; ^1H NMR (500 MHz, DMSO-d_6, Figure S2) δ (ppm) 2.54 (m, 4H relative integration), 2.90−2.80 (m, 6H), 3.11 (m, 4H) 3.38 (m, 20H), 8.29−7.58 (m, 8H).

Analysis. The molecular weight of PFT was measured by gel permeation chromatography (GPC) prior to quaternization of the amine group using *N*,*N*-dimethylformamide (DMF) as the solvent and polystyrene as the standard. Two different batches were synthesized in order to study the effects of the degree of polymerization on the self-assembly. The shorter polymer had a number average molar mass M_n = 10 530 g/mol and a weight average molar mass M_w = 21 300 g/mol, yielding a polydispersity index of M_w/M_n = 2.02. The molar mass of the polymer as determined by GPC, combined with the molar mass of a single repeat unit (446.69 g/mol), translates to a degree of polymerization between 24 (number weighted) and 48 (mass weighted). Using Cambridgesoft's Chem3D Ultra 11.0.1 to model a PFT trimer,[106] the average length of a monomer unit was 12.4 Å, meaning that an elongated polymer chain would have an average length of approximately 30 nm (number weighted) or 60 nm (mass weighted). The longer polymer was approximately twice as long, having M_n = 20 000 and M_w = 35 000 for a PDI = 1.75 and length of ∼60 nm (number weighted) or 105 nm (mass weighted).

All solution-phase photophysics and scattering measurements were carried out on samples made by dissolving solid polymer samples in the appropriate solvent by stirring and heating to no more than 70 °C. Water was deionized to 18 MΩ·cm and filtered using a Millipore 4-bowl Super-Q system. Then, 200 proof ethanol (EtOH) was used as received from Gold Shield Chemical Company. Solvents used for scattering experiments were filtered using 0.45 μm polyvinylidene fluoride (PVDF) syringe filters. For visible light scattering and spectroscopy, the samples were transferred to 10 mm path length, 3.5 mL quartz cuvettes for measurement. PFT thin films were prepared on glass or quartz substrates that were cleaned by ultrasonication in an Alconox bath for 20 min and rinsed with deionized water.

UV/visible absorption measurements were conducted on a Perkin-Elmer Lambda 25 spectrometer. Photoluminescence (PL) measurements were carried out using a Jobin Yvon Horiba Fluorolog-3 spectrofluorometer in front-face geometry. Light scattering measurements were recorded with a Beckman Coulter N4 Plus submicrometer particle size analyzer using a 10 mW He−Ne laser operating at 632.8 nm.

Small-angle X-ray scattering (SAXS) experiments were conducted at the Stanford Synchrotron Radiation Laboratory (SSRL) Beamline 4-2. Using a syringe pump, 25 μL of each sample was loaded in a quartz capillary and held at 25 °C. Scattered X-rays (λ = 1.38 Å) were collected with a MarCCD detector (sample to detector distance = 2.5 m) and converted to 512 × 512 pixel images. The two-dimensional data were radially averaged to obtain one-dimensional scattering curves. The radially averaged distance distribution function, $P(r)$, was calculated as the inverse Fourier transform of the scattered intensity as a function of scattering vector q. The data were analyzed with the ATSAS package.[107−109]

Atomic force microscopy (AFM) was carried out using a Nanoscope V Dimension 5000 (Bruker Nano, Inc.) in ambient conditions. Phosphorus n-doped silicon cantilevers (MPP-22100, Bruker Nano, Inc.) with spring constants of ∼0.9 N/m, first longitudinal resonance frequencies between 31 and 49 kHz, and nominal tip radii of 10 nm were employed in tapping mode. Simultaneous height and phase images were acquired and reproduced from multiple samples, which were prepared by drop-casting 0.01 mg/mL solutions onto freshly cleaved mica. The solutions were composed of a mixed solvent system consisting of 90% 18 MΩ deionized water and 10% ethanol, which was added to aid wetting to produce more homogeneous coverage on the mica substrates. Optimization of deposition conditions was carried out in order to produce samples with both isolated rod-like structural units and bundles of rods. Simple plane fitting of the acquired images[110] enabled subsequent cross sectional analyses of molecular dimensions by analyzing each feature individually and recording statistics of length, width, and height. Reported values demonstrated no significant variation between different samples or cantilever probes. The applied loading force and nominal radius of the cantilever probe tip produced some image

convolution and molecular deformation,[111] generating slight variation in reported molecular dimensions as compared to expected values from molecular modeling and small-angle X-ray scattering.

Rheological properties of polymer gels were measured under ambient conditions using a Rheometrics RFS2 strain-controlled rheometer. The frequency-dependent storage modulus and loss modulus were measured by loading the gels into a cone-and-plate geometry, which ensures a uniform strain field. To prevent unwanted changes in polymer concentration by solvent evaporation, throughout the rheology measurements, we employed a vapor trap.

For electrical measurements, the charged polymer was dissolved in 18 MΩ water at a concentration of 5 mg/mL; the neutral polymer was dissolved in chloroform at a concentration of 5 mg/mL. Both solutions were passed through a 0.45 μm PVDF filter prior to spin-coating. Indium-doped tin oxide (ITO) substrates were cleaned by successive ultrasonication in detergent solution, deionized water, acetone, and finally isopropyl alcohol. The substrates were then subjected to a dry air plasma treatment (200 mTorr, 10 min) prior to spin-coating a thin poly(ethylenedioxythiophene):poly(sulfonic acid) (PEDOT:PSS) layer. The PEDOT:PSS-coated slides were then baked in a nitrogen atmosphere for 20 min. The aqueous solution of charged polymer was spin-cast in air onto the room temperature PEDOT:PSS-covered substrates at 1000 rpm for 60 s, whereas the neutral polymer solution was cast at 5000 rpm for 60 s. All films were then annealed at 150 °C for 20 min in an argon atmosphere and quenched rapidly on a room temperature metal surface prior to depositing the aluminum cathode (100 nm). The current–voltage characteristics were measured in inert atmosphere using a Keithley 2400 source meter.

Conflict of Interest: The authors declare no competing financial interest.

Acknowledgment. This work was supported by the center for Molecularly Engineered Energy Materials (MEEM), an Energy Frontier Research Center funded by the U.S. Department of Energy, Office of Science, Office of Basic Energy Sciences under award DE-SC0001342, and by the NSF under Grants CHE-0527015 and CHE-1112569. Additional support was provided by NSF Grant CHE-0911758 (Y.R.). Portions of this research were carried out in the Nano and Pico Characterization Laboratory in the California NanoSystems Institute - UCLA, and at the Stanford Synchrotron Radiation Laboratory, a national user facility operated by Stanford University on behalf of the U.S. Department of Energy, Office of Basic Energy Sciences. The SSRL Structural Molecular Biology Program is supported by the Department of Energy, Office of Biological and Environmental Research, and by the National Institutes of Health, National Center for Research Resources, Biomedical Technology Program.

Supporting Information Available: NMR spectra of polymers **2** and **3** and additional time-dependent current voltage data are provided. This material is available free of charge *via* the Internet at http://pubs.acs.org.

REFERENCES AND NOTES

1. McNeill, C.; Friend, R. H. Conjugated–Polymer Blends for Optoelectronics. *Adv. Mater.* **2009**, *21*, 3840–3850.
2. Diebel, C.; Dyakonov, V. Polymer–Fullerene Bulk Heterojunction Solar Cells. *Rep. Prog. Phys.* **2010**, *73*, 096401.
3. Lee, K.; Povlichy, L. K.; Kim, J. Recent Advances in Fluorescent and Colorimetric Conjugated Polymer-Based Biosensors. *Analyst* **2010**, *135*, 2179–2189.
4. Sirringhaus, H.; Bird, M.; Zhao, N. Charge Transport Physics of Conjugated Polymer Field-Effect Transistors. *Adv. Mater.* **2010**, *22*, 3893–3898.
5. Martini, I. B.; Craig, I. M.; Molenkamp, W. C.; Miyata, H.; Tolbert, S. H.; Schwartz, B. J. Controlling Optical Gain in Semiconducting Polymers with Nanoscale Chain Positioning and Alignment. *Nat. Nanotechnol.* **2007**, *2*, 647–652.
6. Service, R. F. Outlook Brightens for Plastic Solar Cells. *Science* **2011**, *332*, 293.
7. Schwartz, B. J. Conjugated Polymers as Molecular Materials: How Chain Conformation and Film Morphology Influence Energy Transfer and Interchain Interactions. *Annu. Rev. Phys. Chem.* **2003**, *54*, 141–172.
8. Friend, R. H.; Gymer, R. W.; Holmes, A. B.; Burroughes, J. H.; Marks, R. N.; Taliani, C.; Bradley, D. D. C.; Dos Santos, D. A.; Brédas, J. L.; Lögdlund, M.; *et al.* Electroluminescence in Conjugated Polymers. *Nature* **1999**, *397*, 121–128.
9. Zhou, Q.; Swager, T. M. Method for Enhancing the Sensitivity of Fluorescent Chemosensors: Energy Migration in Conjugated Polymers. *J. Am. Chem. Soc.* **1995**, *117*, 7017–7018.
10. Kim, J.; Levitsky, I. A.; McQuade, D. T.; Swager, T. M. Structural Control in Thin Layers of Poly(*p*-phenyleneethynylene)s: Photophysical Studies of Langmuir and Langmuir–Blodgett Films. *J. Am. Chem. Soc.* **2002**, *124*, 7710–7718.
11. Lovinger, A. J.; Rothberg, L. J. Electrically Active Organic and Polymeric Materials for Thin-Film-Transistor Technologies. *J. Mater. Res.* **1996**, *11*, 1581–1592.
12. Dimitrakopoulos, C. D.; Malenfant, P. R. L. Organic Thin Film Transistors for Large Area Electronics. *Adv. Mater.* **2002**, *14*, 99–117.
13. Burroughes, J. H.; Bradley, D. D. C.; Brown, A. R.; Marks, R. N.; Mackay, K.; Friend, R. H.; Burns, P. L.; Holmes, A. B. Light-Emitting Diodes Based on Conjugated Polymers. *Nature* **1990**, *347*, 539–541.
14. Gustaffson, G.; Cao, Y.; Treacy, G. M.; Klavetter, F.; Colinari, N.; Heeger, A. J. Flexible Light-Emitting Diodes Made from Soluble Conducting Polymers. *Nature* **1992**, *357*, 477–479.
15. Tessler, N.; Denton, G. J.; Friend, R. H. Lasing from Conjugated Polymer Microcavities. *Nature* **1996**, *382*, 695–697.
16. Doan, V.; Tran, V.; Schwartz, B. J. Ultrafast Intensity-Dependent Stimulated Emission In Conjugated Polymers: The Mechanism for Line Narrowing. *Chem. Phys. Lett.* **1998**, *288*, 576–584.
17. Diaz-Garcia, M. A.; Hide, F.; Schwartz, B. J.; Andersson, M. R.; Pei, Q.; Heeger, A. J. Plastic Lasers: Semiconducting Polymers as a New Class of Solid-State Laser Materials. *Synth. Met.* **1997**, *84*, 455–462.
18. Günes, S.; Neugebauer, H.; Sariciftci, N. S. Conjugated Polymer-Based Organic Solar Cells. *Chem. Rev.* **2007**, *107*, 1324–1338.
19. Granstrom, M.; Petritsch, K.; Arias, A. C.; Lux, A.; Andersson, M. R.; Friend, R. H. Laminated Fabrication of Polymeric Photovoltaic Devices. *Nature* **1998**, *395*, 257–260.
20. Brabec, C. J.; Sariciftci, N. S.; Hummelen, J. C. Plastic Solar Cells. *Adv. Funct. Mater.* **2001**, *11*, 15–26.
21. Liang, Y.; Xu, Z.; Xia, J.; Tsai, S.-T.; Wu, Y.; Li, G.; Ray, C.; Yu, L. For the Bright Future—Bulk Heterojunction Polymer Solar Cells with Power Conversion Efficiency of 7.4%. *Adv. Mater.* **2010**, *22*, E135–E138.
22. Campbell, A. J.; Weaver, M. S.; Lidzey, D. G.; Bradley, D. D. C. Bulk Limited Conduction in Electroluminescent Devices. *J. Appl. Phys.* **1998**, *84*, 6737–6746.
23. Sims, M.; Tuladhar, S. M.; Nelson, J.; Maher, R. C.; Campoy-Quiles, M.; Choulis, S. A.; Mairy, M.; Bradley, D. D. C.; Etchegoin, P. G.; Tregidgo, C.; *et al.* Correlation between Microstructure and Charge Transport in Poly(2,5-dimethoxy-*p*-phenylenevinylene) Thin Films. *Phys. Rev. B* **2007**, *76*, 195206(1–12).
24. Kline, R. J.; McGehee, M. D. Morphology and Charge Transport in Conjugated Polymers. *Polym. Rev.* **2006**, *46*, 27–45.
25. Wu, J. J.; Gross, A. F.; Tolbert, S. H. Host–Guest Chemistry Using an Oriented Mesoporous Host: Alignment and Isolation of a Semiconducting Polymer in the Nanopores of an Ordered Silica Matrix. *J. Phys. Chem. B* **1999**, *103*, 2374–2384.
26. Nguyen, T. Q.; Wu, J. J.; Doan, V.; Schwartz, B. J.; Tolbert, S. H. Control of Energy Transfer in Oriented Conjugated Polymer–Mesoporous Silica Composites. *Science* **2000**, *288*, 652–656.

27. Wu, C.-G.; Bein, T. Controlling Carbon Wires in Ordered, Nanometer-Sized Channels. *Science* **1994**, *264*, 1757–1758.
28. Cadby, A. J.; Tolbert, S. H. Controlling Optical Properties and Interchain Interactions in Semiconducting Polymers by Encapsulation in Periodic Nanoporous Silicas with Different Pore Sizes. *J. Phys. Chem. B.* **2005**, *109*, 17879–17886.
29. Molenkamp, W.; Watanabe, M.; Miyata, H.; Tolbert, S. H. Highly Polarized Luminescence from Optical Quality Films of a Semiconducting Polymer Aligned within Oriented Mesoporous Silica. *J. Am. Chem. Soc.* **2004**, *126*, 4476–4477.
30. Clark, A. P.-Z.; Shen, C. K.-F.; Rubin, Y.; Tolbert, S. H. An Amphiphilic Poly(phenylene ethynylene) as the Structure-Directing Agent for Periodic Nanoscale Silica Composite Materials. *Nano Lett.* **2005**, *5*, 1647–1652.
31. Yang, Y.; Lu, Y.; Lu, M.; Huang, J.; Haddad, R.; Xomeritakis, G.; Liu, N.; Malanoski, A. P.; Sturmayr, D.; Fan, H.; *et al.* Functional Nanocomposites Prepared by Self-Assembly and Polymerization of Diacetylene Surfactants and Silicic Acid. *J. Am. Chem. Soc.* **2003**, *125*, 1269–1277.
32. Jenekhe, S. A.; Chen, X. L. Self-Assembled Aggregates of Rod−Coil Block Copolymers and Their Solubilization and Encapsulation of Fullerenes. *Science* **1998**, *279*, 1903–1907.
33. Jenekhe, S. A.; Chen, X. L. Self-Assembly of Ordered Microporous Materials from Rod−Coil Block Copolymers. *Science* **1999**, *283*, 372–375.
34. Ng, M.-K; Yu, L. Synthesis of Amphiphilic Conjugated Diblock Oligomers as Molecular Diodes. *Angew. Chem., Int. Ed.* **2002**, *41*, 3598–3601.
35. Wang, H.; You, W.; Jiang, P.; Yu, L.; Wang, H. H. Supramolecular Self-Assembly of Conjugated Diblock Copolymers. *Chem.—Eur. J.* **2004**, *10*, 986–993.
36. Kim, F. S.; Ren, G.; Jenekhe, S. A. One-Dimensional Nanostructures of π-Conjugated Molecular Systems: Assembly, Properties, and Applications from Photovoltaics, Sensors, and Nanophotonics to Nanoelectronics. *Chem. Mater.* **2011**, *23*, 682–732, and references therein.
37. Xin, H.; Kim, F. S.; Jenekhe, S. A. Highly Efficient Solar Cells Based on Poly(3-butylthiophene) Nanowires. *J. Am. Chem. Soc.* **2008**, *130*, 5424–5425.
38. Tran, H. D.; Li, D.; Kaner, R. B. One-Dimensional Conducting Polymer Nanostructures: Bulk Synthesis and Applications. *Adv. Mater.* **2009**, *21*, 1487–1499.
39. Wu, C. F.; Szymanski, C.; McNeill, J. Preparation and Encapsulation of Highly Fluorescent Conjugated Polymer Nanoparticles. *Langmuir* **2006**, *22*, 2956–2960.
40. Merlo, J. A.; Frisbie, C. D. Field Effect Transport and Trapping in Regioregular Polythiophene Nanofibers. *J. Phys. Chem. B* **2004**, *108*, 19169–19179.
41. Liu, J.; Arif, M.; Zou, J.; Khondaker, S. I.; Zhai, L. Controlling Poly(3-hexylthiophene) Crystal Dimension: Nanowhiskers and Nanoribbons. *Macromolecules* **2009**, *42*, 9390–9393.
42. Briseno, A. L.; Mannsfeld, S. C. B.; Shamberger, P. J.; Ohuchi, F. S.; Bao, Z.; Jenekhe, S. A.; Xia, Y. Self-Assembly, Molecular Packing, and Electron Transport in n-Type Polymer Semiconductor Nanobelts. *Chem. Mater.* **2008**, *20*, 4712–4719.
43. Chen, L. H.; McBranch, D. W.; Wang, H. L.; Helgeson, R.; Wudl, F.; Whitten, D. G. Highly Sensitive Biological and Chemical Sensors Based on Reversible Fluorescence Quenching in a Conjugated Polymer. *Proc. Natl. Acad. Sci. U.S.A.* **1999**, *96*, 12287–12292.
44. Huang, F.; Wu, H.; Cao, Y. Water/Alcohol Soluble Conjugated Polymers as Highly Efficient Electron Transporting/Injection Layer In Optoelectronic Devices. *Chem. Soc. Rev.* **2010**, *39*, 2500–2521, and references therein.
45. Zhong, C.; Duan, C.; Huang, F.; Wu, H.; Cao, Y. Highly Efficient Electron Injection from Indium Tin Oxide/Cross-Linkable Amino-Functionalized Polyfluorene Interface in Inverted Organic Light Emitting Devices. *Chem. Mater.* **2011**, *23*, 4870–4876.
46. Jiang, H.; Taranekar, P.; Reynolds, J.; Schanze, K. Conjugated Polyelectrolytes: Synthesis, Photophysics, and Applications. *Angew. Chem., Int. Ed.* **2009**, *48*, 4300–4316, and references therein.
47. Hoven, C. V.; Garcia, A.; Bazan, G. C.; Nguyen, T.-Q. Recent Applications of Conjugated Polyelectrolytes in Optoelectronic Devices. *Adv. Mater.* **2008**, *20*, 3793–3810.
48. Bunz, U. H. F. Poly(aryleneethynylene)s. *Macromol. Rapid Commun.* **2009**, *30*, 772–805.
49. Häger, H.; Heitz, W. Synthesis of Poly(phenyleneethynylene) without Diyne Defects. *Macromol. Chem. Phys.* **1998**, *199*, 1821–1826.
50. Tan, C. Y.; Pinto, M. R.; Schanze, K. S. Photophysics, Aggregation and Amplified Quenching of a Water-Soluble Poly(phenylene ethynylene). *Chem. Commun.* **2002**, 446–447.
51. Pinto, M. R.; Kristal, B. M.; Schanze, K. S. A Water-Soluble Poly(phenylene ethynylene) with Pendant Phosphonate Groups. Synthesis, Photophysics, and Layer-by-Layer Self-Assembled Films. *Langmuir* **2003**, *19*, 6523–6533.
52. Haskins-Glusac, K.; Pinto, M. R.; Tan, C. Y.; Schanze, K. S. Luminescence Quenching of a Phosphorescent Conjugated Polyelectrolyte. *J. Am. Chem. Soc.* **2004**, *126*, 14964–14971.
53. Kim, I. B.; Dunkhorst, A.; Gilbert, J.; Bunz, U. H. F. Sensing of Lead Ions by a Carboxylate-Substituted PPE: Multivalency Effects. *Macromolecules* **2005**, *38*, 4560–4562.
54. Brookins, R. N.; Schanze, K. S.; Reynolds, J. R. Base-Free Suzuki Polymerization for the Synthesis of Polyfluorenes Functionalized with Carboxylic Acids. *Macromolecules* **2007**, *40*, 3524–3526.
55. VanVeller, B.; Swager, T. M. Biocompatible Post-polymerization Functionalization of a Water Soluble Poly(*p*-phenylene ethynylene). *Chem. Commun.* **2010**, *46*, 5761–5763.
56. Chen, L.; McBranch, D. W.; Wang, H.-L.; Helgeson, R.; Wudl, F.; Whitten, D. G. Highly Sensitive Biological and Chemical Sensors Based on Reversible Fluorescence Quenching in a Conjugated Polymer. *Proc. Natl. Acad. Sci. U.S.A.* **1999**, *96*, 12287–12292.
57. Huang, F.; Hou, L.; Wu, H.; Wang, X.; Shen, H.; Cao, W.; Yang, W.; Cao, Y. High-Efficiency, Environment-Friendly Electroluminescent Polymers with Stable High Work Function Metal as a Cathode: Green- and Yellow-Emitting Conjugated Polyfluorene Polyelectrolytes and Their Neutral Precursors. *J. Am. Chem. Soc.* **2004**, *126*, 9845–9853.
58. Casagrande, T.; Imin, P.; Cheng, F.; Botton, G. A.; Zhitomirsky, I.; Adronov, A. Supramolecular Functionalization of Single-Walled Carbon Nanotubes (SWNTs) with Conjugated Polyelectrolytes and Their Patterning on Surfaces. *Chem. Mater.* **2010**, *22*, 2741–2749.
59. Hodgkiss, J. M.; Tu, G.; Albert-Seifried, S.; Huck, W. T. S.; Friend, R. H. Ion-Induced Formation of Charge-Transfer States in Conjugated Polyelectrolytes. *J. Am. Chem. Soc.* **2009**, *131*, 8913–8921.
60. Lin, C.-Y.; Garcia, A.; Zalar, P.; Brzezinski, J. Z.; Nguyen, T.-Q. Effect of Thermal Annealing on Polymer Light-Emitting Diodes Utilizing Cationic Conjugated Polyelectrolytes as Electron Injection Layers. *J. Phys. Chem. C* **2010**, *114*, 15786–15790.
61. Choi, H.; Park, J. S.; Jeong, E.; Kim, G.-H.; Lee, B. R.; Kim, S. O.; Song, M. H.; Woo, H. Y.; Kim, J. Y. Combination of Titanium Oxide and a Conjugated Polyelectrolyte for High-Performance Inverted-Type Organic Optoelectronic Devices. *Adv. Mater.* **2011**, *23*, 2759–2763.
62. He, C.; Zhong, C.; Wu, H.; Yang, R.; Yang, W.; Huang, F.; Bazan, G. C.; Cao, Y. Origin of the Enhanced Open-Circuit Voltage in Polymer Solar Cells *via* Interfacial Modification Using Conjugated Polyelectrolytes. *J. Mater. Chem.* **2010**, *20*, 2617–2622.
63. Fang, J.; Wallikewitz, B. H.; Gao, F.; Tu, G.; Müller, C.; Pace, G.; Friend, R. H.; Huck, W. T. S. Conjugated Zwitterionic Polyelectrolyte as the Charge Injection Layer for High-Performance Polymer Light-Emitting Diodes. *J. Am. Chem. Soc.* **2011**, *133*, 683–685.
64. Scherf, U. Counterion Pinning in Conjugated Polyelectrolytes for Applications in Organic Electronics. *Angew. Chem., Int. Ed.* **2011**, *50*, 5016–5017.

65. Chi, C. Y.; Mikhailovsky, A.; Bazan, G. C. Design of Cationic Conjugated Polyelectrolytes for DNA Concentration Determination. *J. Am. Chem. Soc.* **2007**, *129*, 11134–11145.
66. Li, H. P.; Bazan, G. C. Conjugated Oligoelectrolyte/ssDNA Aggregates: Self-Assembled Multicomponent Chromophores for Protein Discrimination. *Adv. Mater.* **2009**, *21*, 964–967.
67. Englert, B. C.; Bakbak, S.; Bunz, U. H. F. Click Chemistry as a Powerful Tool for the Construction of Functional Poly(*p*-phenyleneethynylene)s: Comparison of Pre- and Post-functionalization Schemes. *Macromolecules* **2005**, *38*, 5868–5877.
68. Wang, Y.; Park, J. S.; Leeche, J. P.; Miao, S. B.; Bunz, U. H. F. Poly(aryleneethynylene)s with Orange, Yellow, Green, and Blue Solid-State Fluorescence. *Macromolecules* **2007**, *40*, 1843–1850.
69. VanVeller, B.; Miki, K.; Swager, T. M. Rigid Hydrophilic Structures for Improved Properties of Conjugated Polymers and Nitrotyrosine Sensing in Water. *Org. Lett.* **2010**, *12*, 1292–1295.
70. Jiang, H.; Zhao, X.; Schanze, K. S. Effects of Polymer Aggregation and Quencher Size on Amplified Fluorescence Quenching of Conjugated Polyelectrolytes. *Langmuir* **2007**, *23*, 9481–9486.
71. Hoven, C. V.; Yang, R.; Garcia, A.; Heeger, A. J.; Nguyen, T.-Q.; Bazan, G. Ion Motion in Conjugated Polyelectrolyte Electron Transporting Layers. *J. Am. Chem. Soc.* **2007**, *129*, 10976–10977.
72. Hoven, C. V.; Yang, R.; Garcia, A.; Crockett, V.; Heeger, A. J.; Bazan, G.; Nguyen, T.-Q. Electron Injection into Organic Semiconductor Devices from High Work Function Cathodes. *Proc. Natl. Acad. Sci. U.S.A.* **2008**, *105*, 12730–12735.
73. Israelachvili, J. N. *Intermolecular and Surface Forces*, 2nd ed.; Academic Press: London, 1992.
74. Nguyen, T.-Q.; Doan, V.; Schwartz, B. J. Control of Energy Transport in Conjugated Polymers Using an Ordered Mesoporous Silica Matrix. *J. Chem. Phys.* **1999**, *110*, 4068–4078.
75. von Berlepsch, H.; Harnau, L.; Reineker, P. Persistence Length of Wormlike Micelles from Dynamic Light Scattering. *J. Phys. Chem. B.* **1998**, *102*, 7518–7522.
76. Evans, D. F.; Miller, D. D. Part I: A Reappraisal of the Role of Water in Promoting Amphiphilic Assembly and Structure. In *Water Science Reviews 4*; Franks, F., Ed.; Cambridge University Press: London, 1989, pp 1−39.
77. Svergun, D. I.; Koch, M. H. J. Small-Angle Scattering Studies of Biological Macromolecules in Solution. *Rep. Prog. Phys.* **2003**, *66*, 1735–1782.
78. Hugger, S.; Thoman, R.; Heinzel, T.; Thurn-Albrecht, T. Semicrystalline Morphology in Thin Films of Poly(3-hexylthiophene). *Colloid Polym. Sci.* **2004**, *282*, 932–938.
79. Cates, M. E.; Candau, S. J. Statics and Dynamics of Worm-like Surfactant Micelles. *J. Phys.: Condens. Matter* **1990**, *2*, 6869–6892.
80. Polyelectrolyte Gels: Properties, Preparation, and Applications. In *ACS Symposium Series 480*; Harlond, R. S., Prud'homme, R. K., Eds.; American Chemical Society: Washington, DC, 1992.
81. MacKintosh, F. C.; Kas, J.; Janmey, P. A. Elasticity of Semiflexible Biopolymer Networks. *Phys. Rev. Lett.* **1995**, *75*, 4425–4428.
82. Kroy, K.; Frey, E. Force-Extension Relation and Plateau Modulus for Wormlike Chains. *Phys. Rev. Lett.* **1996**, *77*, 306–309.
83. The inflection point was determined by estimating the zero-point in calculated second-order difference quotients in G'.
84. Inoue, T.; Inoue, Y.; Watanabe, H. Nonlinear Rheology of CTAB/NaSal Aqueous Solutions: Finite Extensibility of a Network of Wormlike Micelles. *Langmuir* **2005**, *21*, 1201–1208.
85. Storm, C.; Pastore, J. J.; MacKintosh, F. C.; Lubensky, T. C.; Janmey, P. A. Nonlinear Elasticity in Biological Gels. *Nature* **2005**, *435*, 191–194.
86. Greczynski, G.; Fahlman, M.; Salaneck, W. R.; Johansson, N.; dos Santos, D. A.; Dkhissi, A.; Brédas, J.-L. Electronic Structure of Poly(9,9-dioctylfluorene) in the Pristine and Reduced State. *J. Chem. Phys.* **2002**, *16*, 1700–1706.
87. Onoda, M.; Manda, Y.; Yokoyama, M.; Sugimoto, R.; Yoshino, K. A Photo-electron Emission Study of Polythiophene Derivatives. *J. Phys.: Condens. Matter* **1989**, *1*, 3859–3864.
88. Smith, A. D.; Shen, C. K. F.; Roberts, S. T.; Helgeson, R.; Schwartz, B. J. Ionic Strength and Solvent Control over the Physical Structure, Electronic Properties and Superquenching of Conjugated Polyelectrolytes. *Res. Chem. Intermed.* **2007**, *33*, 125–142.
89. Schaller, R. D.; Snee, P. T.; Johnson, J. C.; Lee, L. F.; Wilson, K. R.; Haber, L. H.; Saykally, R. J.; Nguyen, T.-Q.; Schwartz, B. J. Nanoscopic Interchain Aggregate Domain Formation in Conjugated Polymer Films Studied by Third Harmonic Generation (THG) Near-Field Scanning Optical Microscopy (NSOM). *J. Chem. Phys.* **2002**, *117*, 6688–6698.
90. Schaller, R. D.; Lee, L. F.; Johnson, J. C.; Haber, L. H.; Saykally, R. J.; Vieceli, J.; Benjamin, I.; Nguyen, T.-Q.; Schwartz, B. J. The Nature of Interchain Excitations in Conjugated Polymers: Near-Field Optical Studies of Spatially-Varying Solvatochromism in Annealed MEH-PPV Films. *J. Phys. Chem. B* **2002**, *106*, 9496–9506.
91. Nguyen, T.-Q.; Martini, I. B.; Liu, J.; Schwartz, B. J. Controlling Interchain Interactions in Conjugated Polymers: The Effects of Chain Morphology on Exciton−Exciton Annihilation and Aggregation in MEH-PPV Films. *J. Phys. Chem. B* **2000**, *104*, 237–255.
92. Martini, I. B.; Smith, A. D.; Schwartz, B. J. Evidence for the Direct Production of Interchain Species in Conjugated Polymer Films: The Ultrafast Stimulated Emission and Fluorescence Dynamics of MEH-PPV. *Phys. Rev. B* **2004**, *69* (), 035204(1−12).
93. Spano, F. C.; Clark, J.; Silva, C.; Friend, R. H. Determining Exciton Coherence from the Photoluminescence Spectral Line Shape in Poly(3-hexylthiophene) Thin Films. *J. Chem. Phys.* **2009**, *130*, 074904.
94. Wennerstrom, H.; Lindman, B. Micelles. Physical Chemistry of Surfactant Association. *Phys. Rep.* **1979**, *52*, 1–86.
95. Clark, A. P.-Z.; Cadby, A. J.; Shen, C. K.-F.; Rubin, Y.; Tolbert, S. H. Synthesis and Self-Assembly of an Amphiphilic Poly(phenylene ethynylene) Ionomer. *J. Phys. Chem. B* **2006**, *110*, 22088–22096.
96. Gregg, B. A. Transport in Charged Defect-Rich π-Conjugated Polymers. *J. Phys. Chem. C* **2009**, *113*, 5899–5901.
97. Wang, D.; Kopidakis, N.; Reese, M. O.; Gregg, B. A. Treating Poly(3-hexylthiophene) with Dimethylsulfate Improves Its Photoelectrical Properties. *Chem. Mater.* **2008**, *20*, 6307–6309.
98. Nguyen, T.-Q.; Schwartz, B. J. Ionomeric Control of Interchain Interactions, Morphology and the Electronic Properties of Conjugated Polymer Solutions and Films. *J. Chem. Phys.* **2002**, *116*, 8198–208.
99. Nguyen, T.-Q.; Yee, R. Y.; Schwartz, B. J. Solution Processing of Conjugated Polymers: The Effects of Polymer Solubility on the Morphology and Electronic Properties of Semiconducting Polymer Films. *J. Photochem. Photobiol. A* **2001**, *144*, 21–30.
100. Lampert, M. A.; Mark, P. *Current Injection in Solids*; Academic Press: New York, 1970.
101. Chen, L. H.; McBranch, D. W.; Wang, H. L.; Helgeson, R.; Wudl, F.; Whitten, D. G. Highly Sensitive Biological and Chemical Sensors Based on Reversible Fluorescence Quenching in a Conjugated Polymer. *Proc. Natl. Acad. Sci. U.S.A.* **1999**, *96*, 12287–12292.
102. Dwight, S. J.; Gaylord, B. S.; Hong, J. W.; Bazan, G. C. Perturbation of Fluorescence by Nonspecific Interactions between Anionic Poly(phenylenevinylene)s and Proteins: Implications for Biosensors. *J. Am. Chem. Soc.* **2004**, *126*, 16850–16859.

103. Chemburu, S.; Ji, E.; Casana, Y.; Wu, Y.; Buranda, T.; Schanze, K. S.; Lopez, G. P.; Whitten, D. G. Conjugated Polyelectrolyte Supported Bead Based Assays for Phospholipase A_2 Activity. *J. Phys. Chem. B* **2008**, *112*, 14492–14499.
104. Wang, D.; Gong, X.; Heeger, P. S.; Rininsland, F.; Bazan, G. C.; Heeger, A. J. Biosensors from Conjugated Polyelectrolyte Complexes. *Proc. Natl. Acad. Sci. U.S.A.* **2002**, *99*, 49–53.
105. Hou, J.; Tan, Z.; Yan, Y.; He, Y.; Yang, C.; Li, Y. Synthesis and Photovoltaic Properties of Two-Dimensional Conjugated Polythiophenes with Bi(thienylenevinylene) Side Chains. *J. Am. Chem. Soc.* **2006**, *128*, 4911–4916.
106. PFT trimer modeled using Cambridgesoft ChemBio3D Ultra 11.0.1 MM2 energy minimization using a minimum RMS gradient of 0.1. This structure yielded a much lower total energy (359 kcal/mol) than the alternative structure in which the angles of the fluorene and thiophene monomers augment instead of offset (406 kcal/mol), producing a substantial bend in the polymer backbone.
107. Glatter, O.; Kratky, O. *Small Angle X-ray Scattering*; Academic Press Inc.; London, 1982.
108. Svergun, D. I. Determination of the Regularization Parameter in Indirect-Transform Methods Using Perceptual Criteria. *J. Appl. Crystallogr.* **1992**, *25*, 495–503.
109. Konarev, P. V.; Volkov, V. V.; Sokolova, A. V.; Koch, M. H. J.; Svergun, D. I. PRIMUS: A Windows PC-Based System for Small-Angle Scattering Data Analysis. *J. Appl. Crystallogr.* **2003**, *36*, 1277–1282.
110. Horcas, I.; Fernandez, R.; Gomez-Rodriguez, J. M.; Colchero, J.; Gomez-Herrero, J.; Baro, A. M. WSXM: A Software for Scanning Probe Microscopy and a Tool for Nanotechnology. *Rev. Sci. Instrum.* **2007**, *78*, 013705(1−8).
111. Magonov, S. N. Visualization of Polymers at Surfaces and Interfaces with Atomic Force Microscopy. In *Handbook of Surfaces and Interfaces of Materials*; Nalwa, H. R., Ed.; Academic Press: New York, 2001; Vol. 2, pp 393−429, Chapter 10.